Magneto-optical effects of excitons in BiI_3 crystals under pulsed high magnetic fields: Indirect and direct excitons

S. Takeyama, K. Watanabe,* and N. Miura
Institute for Solid State Physics, University of Tokyo, Roppongi, Minato-ku, Tokyo 106, Japan

T. Komatsu, K. Koike, and Y. Kaifu
Department of Physics, Faculty of Science, Osaka City University, Sumiyoshi-ku, Osaka 558, Japan
(Received 2 May 1989)

Magneto-optical spectra for the exciton transitions near the fundamental absorption edge in BiI_3 crystals were investigated in pulsed high magnetic fields up to 42 T. A remarkable anisotropy was observed in the magneto-optical effects on both the indirect and direct excitons with respect to the relative direction of magnetic field and incident light polarization. It was found that both the energy shift of all the observed excitons and the intensity of field-induced excitons showed a quadratic dependence on magnetic field. The observed magnetic-field effects were interpreted in terms of the characteristic Zeeman effects on small-radius cationic excitons including the $6s^2$-to-$6s6p$ transitions in the cations.

I. INTRODUCTION

The optical properties of insulators and semiconductors in the vicinity of the fundamental absorption edge are governed mainly by exciton transitions. The magneto-optical measurements are a rich source of information on the internal structure of the excitons.[1] For weakly bound Wannier excitons with a large exciton radius, a relatively low magnetic field is sufficient to investigate the internal structure.[2] On the other hand, excitons with strong (Frenkel-type) or intermediate binding usually exhibit a strong absorption band near the fundamental edge with a broad bandwidth, reflecting a strong exciton-phonon interaction. In order to obtain an appreciable magneto-optical effect in such a system, a very high magnetic field is required. It is for this reason that, until now, there have been very few reports on magneto-optical effects on excitons having small radii. BiI_3 is a crystal that possesses excitons with a small radius. However, the excitons in BiI_3 show a sharp threshold step of the transition with an appropriate optical density. Therefore, even a small effect is detectable without using very high fields.

BiI_3 crystals belong to a family of layered metal halides. These materials are composed of strongly bonded two-dimensional *X-M-X* layers which are weakly coupled by the van der Waals force. In BiI_3 crystals the metal ions (M) occupy two-thirds of the octahedral vacant sites surrounded by adjacent halogen (X) planes, and the M plane consists of a honeycomb-like arrangement of Bi ions. There are three different possible positions of the octahedral vacant site. As a result, there are three different types of homeycomb Bi planes, which are named A, B, and C layers. In normal stacking, three layers are successively stacked along the c axis, which forms a conventional hexagonal lattice (large cell). The layer arrangement is $\alpha\beta^A\gamma\alpha\beta^B\gamma\alpha\beta^C\gamma\ldots\ldots$, where α, β, and γ denote the three possible positions of the close-packed atomic site. The primitive cell, which contains two BiI_3 molecules, is a rhombohedron with space group C_{3i}^2.[3] The rhombohedral lattice of such a three-layer structure is called a 3R structure. The ordered stacking of the atomic sheets is due to a long-range force making a uniform distribution of the honeycomb hole (unoccupied site in the M sheet) over the crystal.

Characteristic line shapes of the band-edge exciton spectra in BiI_3 are shown in Fig. 1.[4] The intrinsic absorption edge of the BiI_3 crystal originates from an allowed indirect exciton transition from the valence-band maximum at the Γ point to the conduction-band minimum at the Z point in the Brillouin zone accompanied by three different momentum-conserving A_g-mode optical phonons, called $A(Z)$, $B(Z)$, and $C(Z)$.[5] The indirect exciton energy E_{gx}^i has been determined to be 2.0081 eV at 2 K. The energy position of the indirect exciton transition is close to that of the direct exciton. For that reason, the oscillator strength of the indirect exciton transition is about 10^3 times larger than that in normal indirect semiconductors.[5] Such a large oscillator strength enables the observation of clear steps of the indirect transitions assisted by phonons.

The anisotropic direct exciton transitions have been investigated by reflection spectra using a polarized light. The absorption coefficient was obtained from the Kramers-Krönig transformation of the reflection spectra in a wide wavelength region.[4] The direct exciton transitions were observed at 2.072 eV ($\mathbf{E}\perp\mathbf{z}$, $\mathbf{k}\perp\mathbf{z}$, or $\mathbf{k}\parallel\mathbf{z}$) and 2.08 eV ($\mathbf{E}\parallel\mathbf{z},\mathbf{k}\perp\mathbf{z}$) at 4.2 K with relatively broad bandwidths and strong absorption strength. Here, E is the electronic field of the incident light of which wave vector is k, and the axis z stands for the direction perpendicular to the layer stacking. The absorption spectra in the range from the indirect exciton to the low-energy part of the direct exciton transition can be observed in a sample with

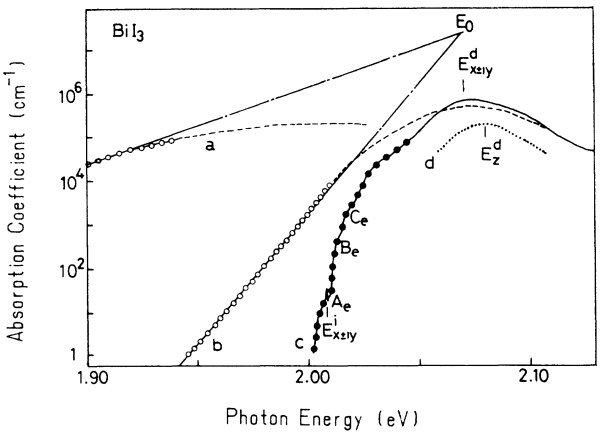

FIG. 1. The absorption spectra around the band-edge excitons in the (E⊥z,k∥z) (solid and dashed lines) and (E∥z,k⊥z) configurations (dotted line). Spectrum *a* is the Urbach tail of the direct exciton at 290 K and spectrum *b* at 77 K, where open circles show the points obtained by the transmission measurements using the several cleaved samples, and dashed lines show the spectra near the direct exciton peak at the same temperatures, which were obtained by a Kramers-Krönig (KK) analysis. The crossing point E_0 of the two lines is the convergent energy in the Urbach rule, which coincides with that of the direct exciton $E^d_{x\pm iy}$. Spectrum *c* shows the wide range of the absorption coefficient from the indirect exciton $E^i_{x\pm iy}$ to the direct exciton peak region, where A_e, B_e, and C_e denote the phonon emission steps of the indirect exciton transition conserving their momenta in the transition with the A_g-mode optical phonons, $A(Z)$, $B(Z)$, and $C(Z)$. Solid circles are those obtained from transmission measurements in as-grown and cleaved thin samples. The solid line shows the spectrum obtained by the KK analysis of the reflection spectrum in (E⊥z,k∥z). *d* shows the spectrum of the direct exciton peak E^d_z region obtained by the KK analysis of the reflection spectrum in (E∥z,k⊥z).

a proper thickness which is obtained by successive cleaving. At low temperatures near 4.2 K, the low-energy tail of the absorption edge is an indirect type. At higher temperatures above 60 K, the tail is dominated by an Urbach tail of the direct transition.[6] These behaviors at 77 and 290 K are shown in Figs. 1(b) and 1(a), respectively.

Cations in BiI_3 crystals have the valence electron configuration $6s^2$, which is the same as Tl^+ and Pb^{2+} ions. According to band-structure calculations,[7] the uppermost valence band is composed of $6s^2$ electrons in Bi^{3+} and the lowest conduction band mainly originates from the *p*-like orbit of Bi^{3+}. Thus the exciton transition in BiI_3 is considered to be "cationic" due to *s-p* transitions within the cation. The anisotropic exciton transition observed in the reflection spectra has been interpreted by the cationic exciton model.[6] In this model, the exciton states consist of twelve states arising from an *s* hole and a *p* electron in an anisotropic crystalline field Δ_c including a large Coulomb, exchange, and spin-orbit interactions. All the parameters in the model have been evaluated by fitting the observed transition energy and the intensity. The band-edge exciton states are composed of four states of the triplet origin with an admixture of some singlet components caused by the spin-orbit interactions. The prominent exciton absorption band at 2.072 eV (allowed for E⊥z) and the weak absorption band at 2.08 eV (E∥z) correspond to degenerate ψ_6 [$(x+iy)$-like] and ψ_{10}[$(x-iy)$-like] states and to ψ_3(z-like) state, respectively. The ψ_4 state has an almost triplet character, and is therefore optically forbidden. More detailed explanations of the states in the cationic exciton model including the symbols are given in the following sections. A large Coulomb interaction of the cationic excitons in BiI_3, which leads to a small radius of the relative motion, has been confirmed by optical experiments.[8]

There have been a few reports on magnetic-field effects of absorption spectra in BiI_3. A study of magnetoabsorption (MA) spectra near the fundamental absorption edge in BiI_3 has been carried out at room temperature by Kolosyuk, Vashchenko, and Berezdetskii.[9] From the large shift of the absorption edge [42 meV/T (B⊥z), 24 meV/T(B∥z)], they concluded that the effective masses of the electron and hole bands for the indirect band-to-band transition are considerably small. In a previous paper[10] we have reported that the MA spectra of the stacking-fault exciton lines are well interpreted by a model based on the linear Zeeman effect of the cationic exciton perturbed by a stacking-fault potential. Preliminary results of MA spectral measurements for the indirect exciton have also been presented.[11]

In this paper, we present more detailed experimental results of the MA spectra of the band-edge excitons observed in BiI_3. The strong polarization dependence and large anisotropies are discussed in terms of the Zeeman effects of cationic excitons having small radii. A qualitative explanation of the magnetic-field effects on the cationic excitons is given by a perturbation approach.

II. EXPERIMENTAL PROCEDURE

BiI_3 powder was synthesized by a reaction of iodine with bismuth in a sealed Pyrex tube and was purified by sublimation in vacuum several times.[12] The purities of both elements were better than 99.9999%. Single crystals were grown by a sublimation method under a condition of excess iodine as a carrier gas. In the MA measurements for the band-edge excitons, thin flake-like crystals with very flat surfaces were selected from as-grown single crystals of good quality. In the measurements of the absorption spectra, only the k∥z configuration was possible.

The MA spectra were measured in high magnetic fields up to 42 T produced by a pulse magnet made of Cu-Nb/Ti superconducting wires to gain mechanical strength. The magnet was immersed in liquid N_2 and energized by a 16-mF, 5-kV condenser bank (200 kJ).[13] A light source is a flash xenon lamp (FXS-T1016, 12 mm diameter, 40 mm length) energized by a 600-μF, 500-V, 750-J condenser unit. The time duration was varied between 1 and 5 ms by changing the inductance connected in series to the lamp. The light from the xenon lamp was introduced to the sample holder by a bundle of fine optical fibers of SiO_2 with a diameter of 200 μm. The total diameter of the bundle with 50 fibers was 1 mm. The

light was further led to the sample in a liquid He bath by a thick optical fiber of 2 mm diameter. The light transmitted through the sample was reflected back to the top of the sample holder by a small prism together with a polarizer (Polaroid sheet). From the top of the sample holder, the light was further transferred by the same kind of fiber bundle to a spectrometer (Narumi RM-L21). The block diagram of the entire experimental setup including the OMA detecting system is shown in Fig. 2. The details of the sample holder for ($\mathbf{B}\|\mathbf{z},\mathbf{k}\|\mathbf{z}$) and ($\mathbf{B}\perp\mathbf{z},\mathbf{k}\|\mathbf{z}$) configurations are shown in the lower part of Fig. 2.

The spectrometer was 1000 mm in focal length, 8.0 Å/mm in inverse dispersion, and $F/7.6$ (at 6000 Å) in aperture. The grating (Bausch and Lomb) mounted in the spectrometer was of 102×102 mm^2, 1200 grooves/mm with a blaze wavelength 5000 Å. The width of an entrance slit was kept about 0.2 mm, which corresponds to the spectral bandwidth of 1.6 Å. The effective aperture of the fiber attached to the entrance slit was $F/5$, which is sufficient to cover the dispersion angle of the spectrometer. Spectra at the exit of the spectrometer were focused onto a diode detector array (700-channel diode units with image intensifiers, the sensitive spectral range 2500 to 9000 Å; EG & G Princeton Applied Research Co., model 1420). The spectral resolution considering the finite size of the diode was 0.7 Å. The resolution is defined as the minimum interval between the two lines which can be resolved. On the other hand, the wavelength at a sharp absorption edge or the absorption peak was able to be determined with an accuracy better than 0.2 Å.

The spectral data obtained were processed by an OMA-II system (EG & G Princeton Applied Research Co.). As shown in Fig. 3, the time duration of the magnetic field pulse was 8 ms, and the gate of the OMA and the flash light were started at the top of the magnetic field. The signal of the magnetic field was taken by a pickup coil wound near the sample, and the pickup coil constant was calibrated to an accuracy of 1%. The variation of the magnetic field during the gate (1 ms) was less

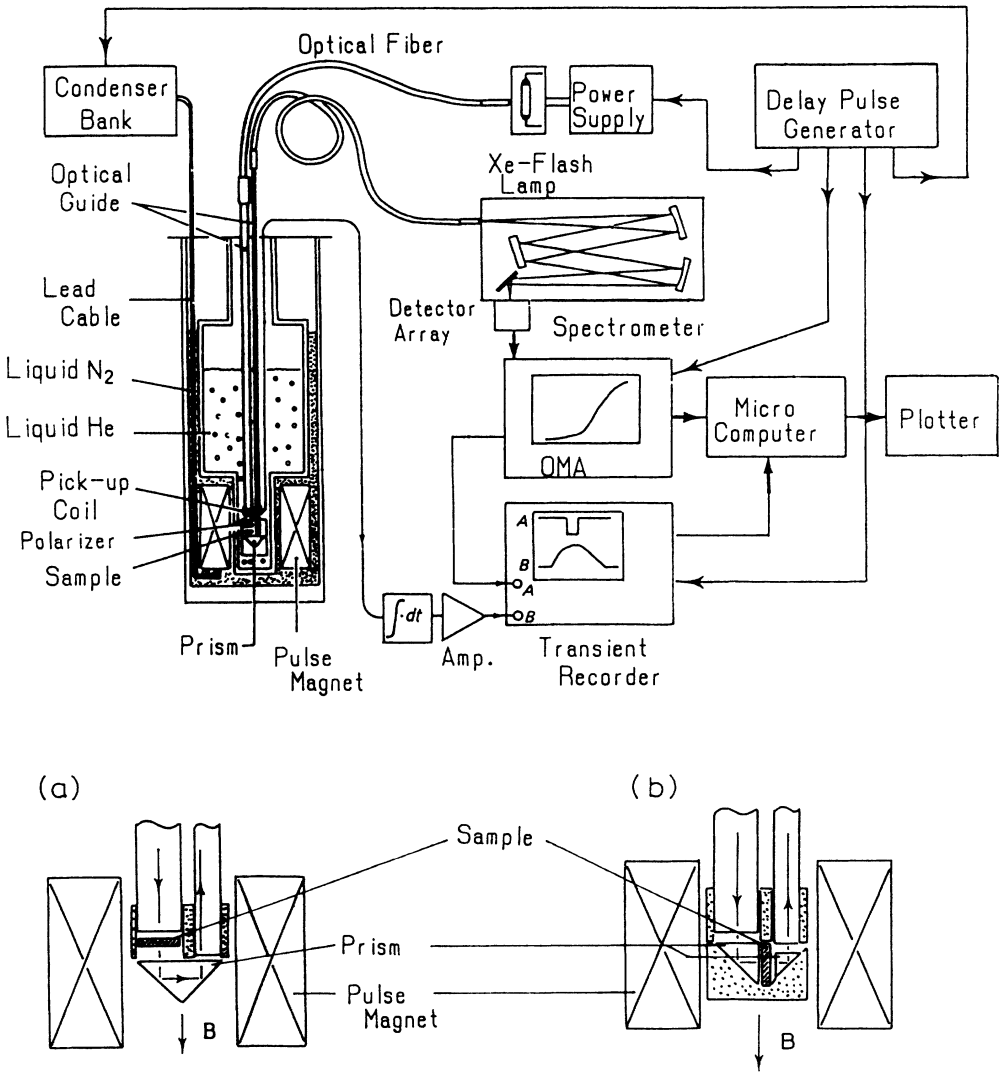

FIG. 2. Block diagram of the magneto-optical measurement system. The enlarged figures of the sample holder are shown for the (a) ($\mathbf{B}\|\mathbf{z},\mathbf{k}\|\mathbf{z}$) and (b) ($\mathbf{B}\perp\mathbf{z},\mathbf{k}\|\mathbf{z}$) configurations

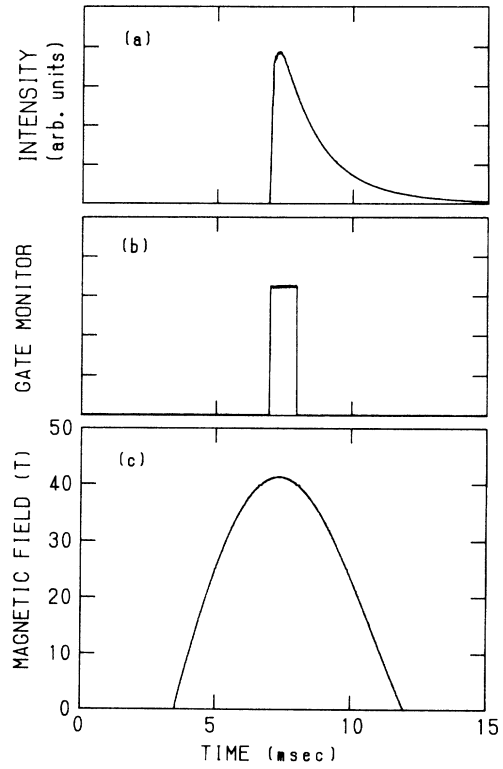

FIG. 3. Experimental traces of the three pulses, showing their relative timing: (a) an incident light source, (b) the OMA gate, and (c) the magnetic field.

than 2% of the maximum magnetic field (i.e., 0.8 T at 40 T). The samples were immersed in a liquid nitrogen or helium bath in the cryostat in which the pulse magnet was installed in a liquid nitrogen bath. The sample temperature was monitored by a calibrated AuFe:Chromel thermocouple placed in the vicinity of the sample.

III. EXPERIMENTAL RESULTS

A. Magneto-absorption spectra of the indirect exciton

The MA spectra around the indirect exciton edge were measured at 4.2 K under pulsed magnetic fields up to 42 T. The MA spectra strongly depend on the magnetic field direction with respect to the crystalline axis or the direction of the E vector of the polarized incident light. The MA spectra at 4.2 K in the $(\mathbf{B}\perp\mathbf{z},k\|\mathbf{z})$ configuration are shown in Fig. 4 for different magnetic fields. The right side of the figure shows the magnetic-field dependence of the MA spectra around the indirect exciton energy E_{gx}^{i} in the $\mathbf{B}\perp\mathbf{E}$ configuration. The A_e step is the indirect exciton transition assisted by the emission of the A_g-mode optical phonon called $A(Z)$ at the Z point in the Brillouin zone. In this configuration, this step shifts to the lower-energy side with increasing magnetic field. The left side of the figure shows the magnetic-field dependence of the MA spectra below the indirect exciton edge in the $\mathbf{E}\|\mathbf{B}$ configuration. The phonon-emission step A_e in this configuration shifts to the higher-energy side, contrary to the $\mathbf{B}\perp\mathbf{E}$ case. It becomes clear from such polarization characteristics as shown in Fig. 4 that the A_e step splits into two thresholds, A_{e1} and A_{e2}, under magnetic fields in the $(\mathbf{B}\perp\mathbf{z},k\|\mathbf{z})$ configuration. This result leads to a conclusion that the indirect exciton splits into two states under magnetic fields. On the other hand, in the $(\mathbf{B}\|\mathbf{z},\mathbf{k}\|\mathbf{z})$ configuration, no detectable shift or splitting of the indirect exciton edge was observed within the available magnetic field. The spectra shown in Fig. 4 also exhibit the P transition. The origin of the P transition has been ascribed to the exciton transition due to

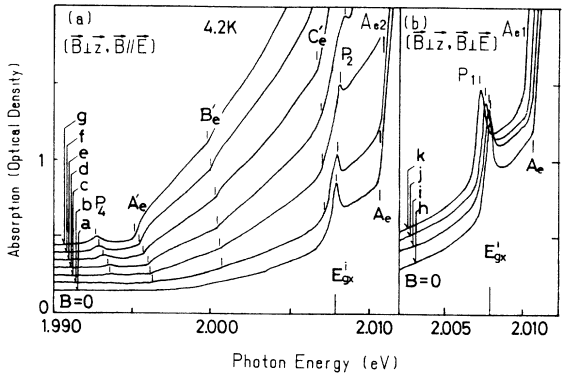

FIG. 4. The MA spectra measured with a polarized light around the indirect exciton absorption edge in the $(\mathbf{B}\perp\mathbf{z},\mathbf{k}\|\mathbf{z})$ configuration at 4.2 K. (a) $\mathbf{B}\|\mathbf{E}$: spectrum a, $B=0$ T; spectrum b, 11.3 T; spectrum c, 15.8 T; spectrum d, 22.2 T; spectrum e, 29.5 T; spectrum f, 35.9 T; spectrum g, 41.0 T; (b) $\mathbf{B}\perp\mathbf{E}$: spectrum h, $B=0$ T; spectrum i, 15.1 T; spectrum j, 28.4 T; spectrum k, 40.1 T.

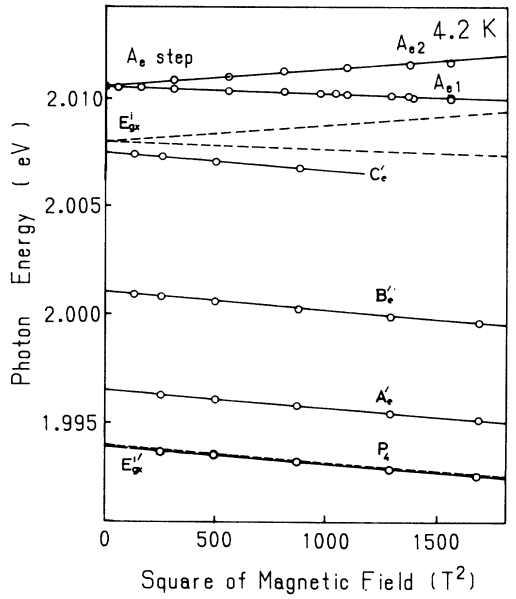

FIG. 5. Magnetic-field dependence of the threshold energies of the indirect exciton transition A_e and the magnetic-field-induced indirect exciton transitions A_e',B_e',C_e' phonon steps. The energy positions for E_{gx}^{i} and $E_{gx}^{i'}$ are also shown by dashed lines. These positions are obtained by subtracting the $A(Z)$ phonon energy from that of the A_e and A_e' steps.

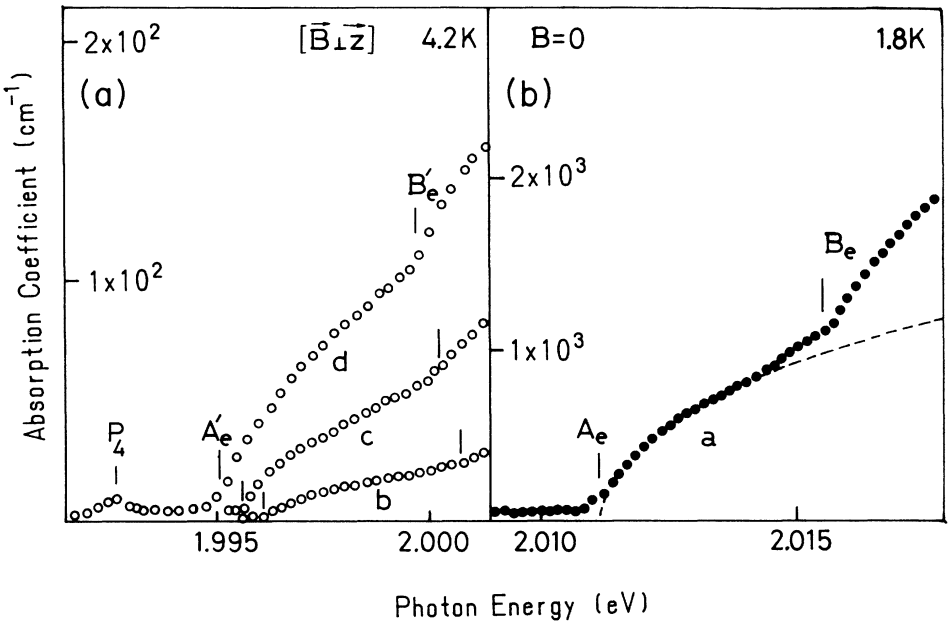

FIG. 6. (a) MA spectra of the field-induced indirect exciton around the A_e' phonon step obtained by subtracting the zero-field spectrum from each spectrum in a magnetic field. (b) Spectrum of the indirect exciton transition around the A_e phonon step in the absence of a magnetic field.

polytype-stacking disorders contained slightly in the crystals.[14] We plan to report the details of the magneto-optic effect for the P line in a future paper.

A drastic change in the MA spectra with increasing magnetic field can be seen in the lower-energy region of the indirect transition in the $\mathbf{B}\|\mathbf{E}$ configuration. In Fig. 4(a), new transition steps denoted as A_e', B_e', and C_e' become clear with increasing magnetic field, where each threshold energy is indicated by vertical bars. The new transition steps induced by the magnetic field have been measured with unpolarized light.[11] The transitions have been assigned as the indirect exciton transitions of the triplet state, which become allowed by a mixture of the singlet state under magnetic fields. Another field-induced step A_a' of the phonon-assisted transition involving the absorption process of the same $A(Z)$ phonon has been observed in thick samples at higher temperatures.[11] The present experimental results indicate that the field-induced indirect transition is allowed only in the $\mathbf{B}\|\mathbf{E}$ configuration. The step A_e' shifts to the lower-energy side with increasing magnetic field. It is noted that the A_e' and B_e' steps at 41.0 T lie at 1.9951 and 1.9997 eV, respectively, in the spectrum g of Fig. 4. The energy difference between B_e' and A_e' is 4.6 meV, which coincides with the energy difference between $B(Z)=7.2$ meV and $A(Z)=2.6$ meV phonons. For the A_e' and C_e' steps, the energy difference corresponds to that between the $C(Z)=13.6$ meV and $A(Z)$ phonons. The energy shift of these thresholds with increasing magnetic field does not show any simple linear dependence on the field strength. The magnetic-field dependence of each threshold energy is plotted in Fig. 5 as a function of B^2. The dependence of the E_{gx}^{i} and the field-induced indirect exciton $E_{gx}^{i'}$ are also given in the figure. From Fig. 5, it is suggested that the energy shift of the transitions with increasing magnetic field is almost proportional to B^2 in the $\mathbf{B}\perp\mathbf{z}$ configuration.

In Fig. 6, the MA spectra around the A_e' phonon step of the field-induced indirect transition are shown in comparison to the spectra around the A_e step of the indirect transition at $B=0$. The MA spectra are obtained by subtracting the zero-field spectrum from the spectra under magnetic fields. A common feature of the line shape can be seen in both indirect ($B=0$) and field-induced transitions. The field-induced transition has a characteristic shape of the allowed indirect exciton transitions ($B=0$). Figure 7 shows the magnetic-field dependence of the absorption intensity of the field-induced exciton transition. Here the intensity was obtained by subtracting the zero-field spectrum from the spectrum around the A_e' step. The dashed line in the figure is a fitting curve calculated by using (7) in Sec. IV A 2.

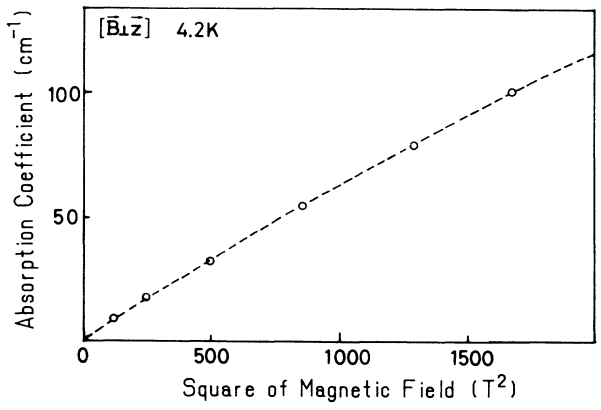

FIG. 7. Magnetic-field dependence of the absorption intensity of the field-induced indirect transition. The value of absorption coefficients is taken at the energy point beginning of the B_e phonon step.

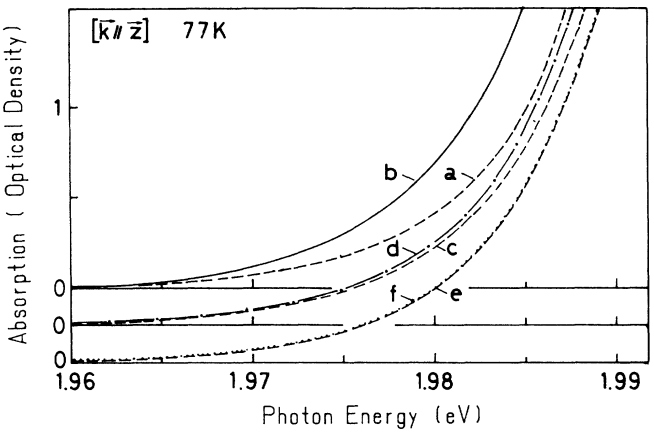

FIG. 8. The MA spectra of the Urbach tail of the direct excitons in different configurations of the magnetic field and electric field of the polarized light at 77 K; spectra *a*, *c*, and *e* (dashed lines) are at $B=0$ T; spectrum *b*, in ($\mathbf{B}\perp\mathbf{z},\mathbf{k}\parallel\mathbf{z},\mathbf{B}\parallel\mathbf{E}$) configuration at 40.0 T; spectrum *d*, in the ($\mathbf{B}\perp\mathbf{z},\mathbf{k}\parallel\mathbf{z},\mathbf{B}\perp\mathbf{E}$) configuration at 40.0 T; spectrum *f*, in the ($\mathbf{B}\parallel\mathbf{z},\mathbf{k}\parallel\mathbf{z}$) configuration measured with an unpolarized light at 40.0 T.

B. Magneto-absorption spectra in the Urbach tail of the direct exciton

Since the absorption coefficient of the direct exciton is extremely large ($\sim 8\times 10^5$ cm^{-1}), the measurement of the absorption spectrum near the energy region of the direct exciton peak for single crystals is difficult in the present system. Therefore, we performed measurements of the MA spectra in the Urbach tail region associated with the direct exciton. As shown in Fig. 1, the log plot of the absorption coefficient gives a straight line in the range 1 to 10^4 cm^{-1} at 77 K, and its linear extrapolation crosses with the line at room temperature at a point E_0 corresponding to the direct exciton energy. Since it is expected that the MA spectra of the Urbach tail show similar polarization dependence to indirect transitions, we examined the polarization dependence in more detail. Figure 8 shows the MA spectra of the Urbach tail in the $\mathbf{B}\parallel\mathbf{E}$ and $\mathbf{B}\perp\mathbf{E}$ configurations. The magnetic field induces a shift of the Urbach tail toward the lower-energy side. The amount of the shift in the $\mathbf{B}\parallel\mathbf{E}$ configuration is larger than that in $\mathbf{B}\perp\mathbf{E}$: The shift at 40 T was -2.8 meV in $\mathbf{B}\parallel\mathbf{E}$ and -0.5 meV in $\mathbf{B}\perp\mathbf{E}$ configurations, respectively. In the case of an unpolarized light, the shift was -1.6 meV. The energy shift of the Urbach tail was found to show nearly B^2 dependence in both configurations. On the other hand, no detectable shift can be observed in the ($\mathbf{B}\parallel\mathbf{z},\mathbf{k}\parallel\mathbf{z}$) configuration as shown by *e* and *f* in Fig. 8.

IV. DISCUSSION

A. Indirect exciton transitions

1. *The magnetic-field dependence of the indirect exciton states*

The indirect exciton transition has been known to be an allowed transition from its characteristic step line shape. Therefore, the indirect exciton states at 2.0079 eV at 4.2 K are considered to have a spin singlet exciton component. A remarkable anisotropy of the magnetic-field effect on the excitons was observed between the $\mathbf{B}\parallel\mathbf{z}$ and the $\mathbf{B}\perp\mathbf{z}$ configurations. Since the shifts and splitting of the indirect exciton transitions were not detected in the $\mathbf{B}\parallel\mathbf{z}$ configuration, it seemed that the diamagnetic shift and the effective g value $g^{\parallel}_{\rm eff}$ were very small. In the $\mathbf{B}\perp\mathbf{z}$ configuration, on the other hand, the indirect exciton states split clearly into two states under magnetic fields. This suggests that the indirect exciton state should be degenerate at zero magnetic field. New exciton transitions under magnetic fields are called magnetic-field-induced indirect exciton.[11] The energy position of the induced exciton obtained by extrapolation to zero magnetic field is 1.9939 eV at 4.2 K. It is considered that the induced transition originates from a mixing of a singlet and pure triplet state resulting from the Zeeman effect. We suppose that one of the indirect states ψ^i_l with a singlet component lies at a higher energy E^i_l than E^i_m of another state ψ^i_m, where the superscript i refers to the indirect exciton states and subscripts l and m to two different states, respectively. The energy shift and the intensity of the transition in magnetic fields can be obtained on the basis of a perturbation approach if the Zeeman matrix element of an off-diagonal component among these two states has a nonzero value. The wave function in a magnetic field is given to a first-order approximation by

$$\psi^i_m(B)=\psi^i_m(B=0)+[|H_{lm}|/(E^i_l-E^i_m)]\psi^i_l+\cdots . \quad (1)$$

The energy, retaining second-order terms, is given by

$$E_m(B)=E_m(B=0)+|H_{lm}|^2/(E^i_m-E^i_l)+\cdots , \quad (2)$$

where H_{lm} is the Zeeman matrix element between l and m states:

$$H_{lm}=\langle\psi_m|H_{\rm Zeeman}|\psi_l\rangle . \quad (3)$$

On the basis of the above model, it is expected that the energy shift is governed by the energy difference between the two states and is proportional to the square of magnetic field. Furthermore, the sign of the shift is determined by the relative energy positions of the two states. On the other hand, the transition intensity of the triplet exciton state is calculated by the following equation:

$$I^i_m(B)=|\langle\psi^i_m(B)|\hat{\pi}\cdot\mathbf{r}|\psi_g\rangle|^2$$
$$=[\pi_r g_{\rm eff}\beta B/(E_m-E_l)]^2 , \quad (4)$$

where $\mathbf{r}$ is the dipole operator, $\hat{\pi}$ is a unit vector of the incident light polarization, $g_{\rm eff}$ is the effective g value for an exciton, β is a Bohr magneton for an electron, and ψ_g is the crystal ground state. Thus the theory predicts that the transition intensity of the exciton is proportional to the square of magnetic field. As shown in Fig. 7, the behavior expected by such second-order perturbation of linear Zeeman terms was actually observed in the indirect transition under magnetic fields. If the mixing occurs between the singlet and triplet states, it is expected that the absolute values of the energy shift of the two states are the same. Actually, as shown in Fig. 5 the high-energy

step of the indirect exciton (A_{e2}) shift to a higher energy by the rate $+1.1$ meV/(40 T)^2, while the field-induced indirect exciton edge at 1.9965 eV (A_e') shifts to a lower energy by the rate -1.0 meV/(40 T)^2. The lower-energy step of the indirect exciton (A_{e1}) shifts to lower energy by the rate -0.6 meV/(40 T)^2, therefore, an undetected partner of the A_{e1} step should exist somewhere in the higher-energy region. The energy difference between the two mixed states can be also roughly evaluated to be 24 meV. Thus the energy of the partner state of the A_{e1} is predicted to be 2.032 eV. Consequently, the indirect exciton states consist of at least four states. Furthermore, we obtained the effective g value of the indirect exciton in the $\mathbf{B}\perp\mathbf{z}$ configuration, as $g_{\text{eff}}^{\perp}=1.6$.

As described above, the characteristic behavior of the magnetic-field effect on indirect excitons can be explained using the perturbation method including the linear Zeeman effects. The validity of this model, however, depends on the nature of the real exciton basis functions in the present material. A model of cationic excitons in BiI_3 predicts the $6s^2$-to-$6s6p$ transition of cations in a unit cell.[10] A brief interpretation of the exciton states is given as follows.

The cationic exciton states in one molecule consist of 12 different eigenstates at the Γ point. The p-electron states are split to p_z and $p_{x\pm y}$ orbitals by an anisotropic crystal field. The electrons and holes bound by a Coulomb interaction construct exciton states, and the exchange interaction between electrons and holes makes each state split into one spin singlet and threefold-degenerate spin triplet states. A large spin-orbit interaction due to the heavy metal mixes the triplet and singlet states belonging to the same irreducible representation in the C_{3i} group of the BiI_3 molecule. As a result, the band-edge excitons are composed of four states of triplet origin. Three of them are optically allowed by a mixture of a singlet component. It may be considered that the exciton states are constructed by a bonding and an antibonding orbital of each cation contained in a unit cell belonging to the C_{3i}^2 symmetry in BiI_3 crystals. Accordingly, the exciton orbit is confined in one unit cell, which is consistent with the large binding energy estimated as 180 meV in BiI_3.[8] Since the unit cell has two BiI_3 molecules, the exciton states consist of 24 states. The band-edge excitons are composed of four (ψ_3^d, ψ_6^d, ψ_{10}^d, and ψ_4^d) bonding states: ψ_3^d (z-like) is allowed optically for $\mathbf{E}\|\mathbf{z}$ polarization, ψ_6^d ($x+iy$-like) and ψ_{10}^d ($x-iy$-like) are allowed for $\mathbf{E}\perp\mathbf{z}$ polarization, and ψ_4^d (pure triplet) is forbidden completely except for the presence of the applied magnetic field.

The model is applicable for long-wavelength excitons ($K=0$: Γ exciton), i.e., in the case of the direct band-edge excitons. The bulk band-edge exciton energy has been experimentally determined to be $E_3=2.08$ eV and the degenerate states E_6 and E_{10} 2.072 eV at 4.2 K by measuring the reflection spectra with polarized light. The indirect exciton energy has been determined to be 2.0081 eV in $\mathbf{E}\perp\mathbf{z}$ configuration, and the transition occurs from the Γ point to the Z point in the Brillouin zone.[5] Since the indirect excitons have a large wave vector, the present cationic exciton model may not necessarily be an appropriate approximation for describing the indirect excitons in principle. However, the irreducible representation of the C_{3i} group at the Z point is the same as that at the Γ point.[15] Therefore, we can assume that the present model is still valid for indirect excitons in practice. The experimentally observed indirect exciton states in magnetic fields correspond well to four of the cationic states. In the indirect exciton case, it is necessary to change the parameters included in the model. The $E_{gx}^{i'}$ (1.9939 eV) state corresponds to ψ_4^i, and the degenerate indirect exciton state at 2.0081 eV to the ψ_6^i and ψ_{10}^i states, respectively. The ψ_3^i state may correspond to the state at 2.032 eV estimated in the preceding discussion.

From the discussion above, it is found that the triplet state ψ_4^i is mixed mainly with $(x-iy)$-like state ψ_{10}^i in the $\mathbf{B}\|\mathbf{E}$ configuration, and the z state ψ_3^i with $x+iy$-like state ψ_6^i in the $\mathbf{B}\perp\mathbf{E}$ configuration. Furthermore, the mixing under magnetic fields depends on the angle ϕ between $\mathbf{B}$ and $\mathbf{E}$. The intensity of exciton transitions to the ψ_4^i and ψ_{10}^i becomes maximum at $\phi=0°$, while zero at $\phi=90°$. On the other hand, that for the ψ_3^i and ψ_6^i show opposite angle dependence. The exciton transition in this material is explained well on the basis of the cationic exciton model.

2. *The line-shape analysis of the magnetic-field-induced indirect exciton transitions*

The indirect exciton transition in BiI_3 at zero magnetic field is an allowed type from the analysis of its line shape as mentioned above. The transition intensity has been analyzed by a simple theory of the form[4]

$$\alpha^i(\omega)=\sum_i a_i(\omega-E_{gx}^i-\omega_i)^{1/2}\ , \tag{5}$$

where the coefficients are $a_A=1.5\times10^4$, $a_B=4.5\times10^4$, and $a_C=4.5\times10^4$ cm^{-1}eV$^{-1/2}$ and the phonon energies are $\omega_A=0.026$, $\omega_B=0.071$, and $\omega_C=0.0136$ eV, respectively. The indirect exciton energy at 2 K is determined to be $E_{gx}^i=2.0081$ eV. The transition intensity given by (5) fit to the experimental data only for the A-phonon emission process. Some contributions from the $(\omega-E-\omega_B)^{3/2}$-like dependence had to be considered in the region of the B-phonon emission process above $E=2.019$ eV.[5] Such a $\frac{3}{2}$ power term might be expected due to the allowed band-to-band transition of an indirect type. In such a case, the estimated Coulomb binding energy of the indirect exciton would become a small value. This is, however, quite fictitious, because the binding energy of the present exciton system is known to be very large.[8] Such a deviation from $\frac{1}{2}$ power term should be attributed to the following terms: the k dependence of the exciton-phonon interaction, the $1/\omega$ dependence of the optical matrix element, the energy denominator based on the second-order perturbation in optical process which depends strongly on the relative position between the intermediate and final states, and finally the band nonparabolicity.

In BiI_3, the intermediate state of the indirect transi-

tions is considered to be the direct exciton state which lies 64 meV above the indirect state. In such a case, the energy denominator becomes important for the contribution to the line shape of the indirect exciton in the higher-energy region. General expressions for the energy dependence of the indirect exciton absorption strength have been shown,[16] assuming the Fröhlich-type intraband exciton-phonon interaction and the parabolic band bottom in the indirect exciton. We apply such an expression to the magnetic-field-induced indirect exciton transitions in the following.

Based upon Eq. (19) in Ref. 16, we can calculate the absorption strength at zero field by the following equation. At 4.2 K, we have to consider only a phonon-emission process.

$$\alpha(\Omega_1)=\sum_i G_i^2 C[(\Omega_1-\omega_i)^{1/2}+b\Delta_{mf}(\Omega_1-\omega_i)^{3/2}] \times\{1/[\Delta_{mf}^{1/2}(\Omega_1-\Delta_{mf})^2]\}\ , \qquad (6)$$

where i runs over all phonons associated with the indirect transitions, and $\Omega_1=\omega-E_{gx}^i$, $\omega_1=A(Z)=2.6$, $\omega_2=B(Z)=7.1$, and $\omega_3=C(Z)=13.6$ meV, respectively. C is a constant containing the dipole transition matrix element and Δ_{mf} is the energy separation between the intermediate and the final state of the indirect exciton transition. G is an exciton-phonon coupling constant and b is a constant related to a band dispersion of an electron and a hole. Here, however, we treat this as a fitting parameter and obtain a value of 3 for it. The calculated $\alpha(\Omega_1)$ is shown by the dashed lines for each phonon component in Fig. 9, assuming the direct exciton as the intermediate state of the indirect transition, and adopting the ratio of the exciton-phonon coupling constant for each phonon $G_A^2:G_B^2:G_C^2=1:0.5:2.6$. It can be noted that the fit to experimental data was excellent.

When the magnetic field is applied, the singlet state is mixed into the triplet exciton state by a Zeeman effect; a new channel of the field-induced indirect transitions becomes allowed as shown by dashed lines in Fig. 10. In this process, the intermediate state of the indirect transitions is the ψ_4^d state. The absorption strength of the field-induced exciton can be obtained experimentally by subtracting the spectrum at zero field from the spectra under magnetic fields. The theoretical absorption strength is expressed by

$$\alpha_4^i(\Omega_1',B)=(\delta^2/1+\delta^2)\alpha_4^i(\Omega_1',B=0)\ , \qquad (7)$$

where

$$\alpha_4^i(\Omega_1',B=0)=\alpha(\Omega_1'),\quad \delta=[g_{\rm eff}\beta B/(E_{gx}^1{}'-E_{gx}^i)]\ ,$$

and

$$\Omega_1'=\omega-E_{gx}^{i'}(1+\delta g_{\rm eff}\beta B)\ .$$

The fitting of (7) at a fixed Ω_1' (2.5 meV) to the experimental data of magnetic-field dependence is shown in Fig. 7 by the dashed line. As a result of fitting, the value of $g_{\rm eff}$ is estimated to be 1.6. This value coincides with the one obtained from the energy shifts in the preceding section. The absorption strength of the Ω_1' dependence at different field strength can be also calculated by (7). Assuming Δ_{mf} to be 56 meV, which gives the triplet state energy $E_4^d=2.050$ eV, and also adopting the ratio of the exciton-phonon coupling constant for each phonon $G_A^2:G_B^2:G_C^2=1:0.5:2.3$, the fitting for the absorption intensity of the field-induced exciton between experiment and theory is excellent as seen in Fig. 11. These values of the exciton-phonon coupling constant are in agreement

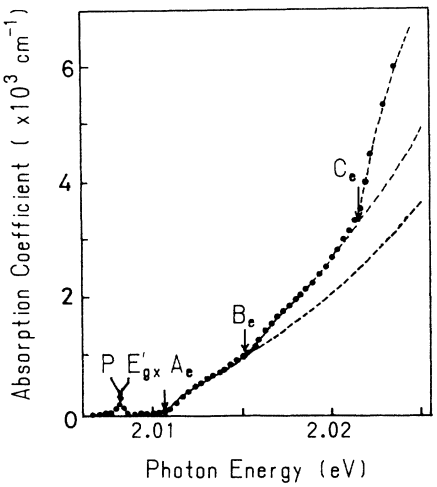

FIG. 9. The line-shape fitting of the indirect exciton transition at 1.8 K in BiI_3 crystal at zero magnetic field. The plot of solid circles shows the absorption coefficient obtained experimentally. The dashed lines are fitting curves calculated for each phonon component by (6) in the text.

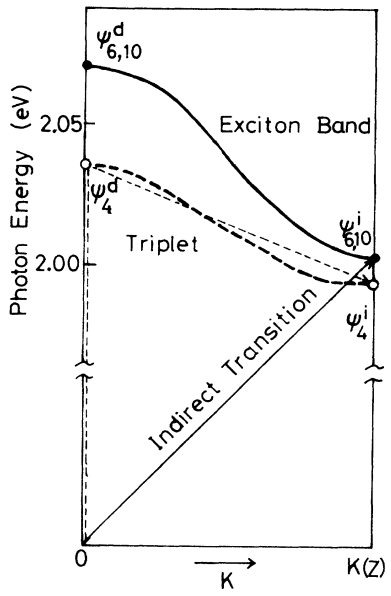

FIG. 10. Energy level scheme of the indirect transition (solid line arrow) and the new transition channel of the field-induced indirect exciton in a magnetic field with their intermediate states at the transitions (dashed line arrow). The exciton dispersion in the k_z direction is shown by a thick solid line and the triplet exciton is shown by a thick dashed line. The ψ_x^j is the state of the direct and indirect excitons j for each cationic states x (see the text).

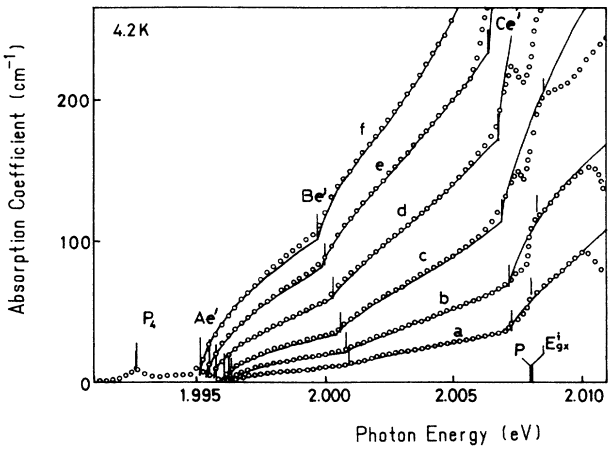

FIG. 11. The MA spectra of the field-induced indirect exciton transitions obtained experimentally by subtracting the zero-field spectrum from that in a magnetic field (○ plots). The solid lines are the fitting curves calculated by Eq. (7) with the parameters given in the text for each magnetic-field strength: spectrum *a*, 11.3 T; spectrum *b*, 15.8 T; spectrum *c*, 22.2 T; spectrum *d*, 29.5 T; spectrum *e*, 35.9 T; spectrum *f*, 41.0 T.

with those obtained for the indirect exciton (at $B=0$) except for a little difference in G_C. In this fitting process, however, we must take the value of the constant b in (6) as about 0.1 times smaller than in the case of zero magnetic field. The reason for this discrepancy may be due to the neglect of another indirect transition channel, such as $\psi^d_{6,10} \rightarrow \psi^i_4$. In this case the intermediate state of the indirect transition to the ψ^i_4 state is both of the direct exciton ψ^d_6 and ψ^d_{10}. The exciton-phonon interaction with an optical phonon is considered to be an interband type. Thus the present analysis based on the simple intraband Frölich interaction gives such a small value of b. The ratio of the coupling constant determined above can be compared with those obtained by another independent experiment of the second-order resonance Raman scattering at the indirect exciton band bottom,[17] which gives the ratio $G^2_A:G^2_B:G^2_C=1:0.5:3.2$. A good agreement was obtained between the two measurements except for the case of the C phonon.

B. Magnetic-field effects on the direct exciton tail

In BiI_3 crystals, at very low temperatures the fundamental absorption edge starts from the phonon-emission steps of the indirect exciton transition and is followed by a direct exciton peak, which lies only 64 meV above the indirect exciton energy. As the temperature is increased, the phonon absorption steps appear, and the absorption intensity below the indirect edge becomes larger. At temperatures higher than 50 K, the phonon steps are smeared out and the first edge is replaced by the tail part of the direct exciton. At 77 K the tail part of the absorption edge consists entirely of an Urbach tail of the direct exciton. The absorption tail at temperatures higher than 77 K is represented by the following equations:

$$\alpha=\alpha_0 \exp[\sigma(E_0-E)/kT] , \tag{8}$$

$$\sigma=(\sigma_0 2kT/\omega_0)\tanh(\omega_0/2kT) , \tag{9}$$

where the parameters are $\alpha_0=3\times10^7$ cm^{-1}, $E_0=2.07$ eV, $\sigma_0=1.02$, and $\omega_0=5.0$ meV. The behavior of the absorption coefficients as a function of photon energy is shown in Fig. 1 for 77 K and 300 K. The parameters above have been determined by the measurements for various samples with different thickness in a wide temperature range.[6]

When a magnetic field is applied in the ($\mathbf{B}\perp\mathbf{z},\mathbf{k}\perp\mathbf{z}$) configuration, the shift of the energy position of the direct exciton and the splitting of degenerate states are expected based on the cationic excitons, as mentioned in Sec. IV A 1. This causes a shift of the Urbach tail of the direct exciton, and a new tail component originating from the triplet state ψ^d_4 grows up with increasing magnetic field. The new tail growth as a consequence of the mixing of a singlet component to a triplet state due to a Zeeman effect may be observed as a low-energy shift of the tail part of the direct exciton, if the triplet state lies close to the direct peak. Moreover, the ψ^d_6 and ψ^d_{10} states split to two peaks, and the ψ^d_6 state shifts to the lower-energy side, which also causes the tail shift to lower energy. Such an expected behavior of the Urbach tail in magnetic fields is consistent with the experimental results. The shift of the Urbach tail to lower energy in the case of an unpolarized light is -1.6 meV at 40 T.

It may be considered from the exciton model that the dependence on the angle between a magnetic field and an electric field of the polarized light is the same as that of the indirect excitons. The peak energy shift in the $\mathbf{B}\perp\mathbf{E}$ configuration is expected towards the lower-energy side and that in the $\mathbf{B}\parallel\mathbf{E}$ towards the higher-energy side, if one does not include the contribution from the triplet state. Our experimental results in the $\mathbf{B}\perp\mathbf{E}$ configuration provided the shift of -0.5 meV at 40 T. The direct exciton peak consists of ψ^d_6 and ψ^d_{10} states. In this configuration, the shift of the tail can be understood by the fact that the energy of the ψ^d_6 state shifts to lower energy by a mixing of other states due to the nonzero Zeeman matrix element. On the other hand, the relatively large shift of -2.8 meV at 40 T with the different sign which is in contrast to the case of the indirect exciton, is obtained in the $\mathbf{B}\parallel\mathbf{E}$ polarized light configuration. In this configuration, the growth of the ψ^d_4 state by a mixing of other singlet components is expected, in addition to the energy shift of the ψ^d_{10} state to the higher-energy side. As the ψ^d_{10} state shifts to the opposite side, the present shift to lower energy may be due to the growth of a singlet component in a triplet exciton. The shift of the tail part in magnetic field depends on whether the triplet state lies at the low- or the high-energy side of the observed energy position. The negative tail shift resulting from the above growth of the peak overcomes the positive shift of the ψ_{10} state. As a result, a low-energy shift of the tail was observed.

The magnetic-field dependence of the Urbach tail can be interpreted by a simple model calculation including the characteristic energy states of the cationic excitons. The Urbach tail in magnetic fields is presented by the following form:

$$\alpha=\sum_m \alpha_m \exp[\sigma(E_m-E)/kT] , \tag{10}$$

where $\alpha_m=\alpha_m(B)$ corresponds to α_0 of each direct exciton state ψ_m^d. From the cationic exciton model, we have only to take $m=4,10$ at $\phi=0°$ and $m=3,6$ at $\phi=90°$. The spectra are calculated by (10) with the following equations:

$$\alpha_3=[|\langle\psi_6^d|H_{\text{Zeeman}}|\psi_3^d\rangle|^2/(E_6-E_3)^2]\alpha_0 , \tag{11}$$

$$\alpha_4=[|\langle\psi_{10}^d|H_{\text{Zeeman}}|\psi_4^d\rangle|^2/(E_{10}-E_4)^2]\alpha_0 , \tag{12}$$

$$\alpha_6=\alpha_0-\alpha_3 , \tag{13}$$

$$\alpha_{10}=\alpha_0-\alpha_4 , \tag{14}$$

where E_m is the energy of each state ψ_m^d at zero field; $E_3=2.08$ eV, $E_4=2.050$, $E_6=E_{10}=2.072$ eV, and $\sigma=0.95$. The calculated and experimental energy shifts of the tail are shown in Fig. 12. On an attempt to fit the experimental shifts, g_{eff} was a fitting parameter varying from 1.0 to 2.0. Excellent agreements were obtained for both angles of $\phi=0°$ and 90° at the value of $g_{\text{egg}}^{\perp}=1.6$. It should be noted this $g_{\text{eff}}^{\perp}$ value coincides with that evaluated for the indirect exciton in the preceding section.

In the ($\mathbf{B}\|\mathbf{z},\mathbf{k}\|\mathbf{z}$) configuration, no detectable shift was observed within the presently available magnetic-field range and the resolution of the spectra, which results in very small value of $g_{\text{eff}}^{\|}$. This shows that the Urbach tail of the direct exciton, therefore the direct exciton itself, has strong anisotropic magnetic-field effects as well as for the indirect excitons, which is consistent with the present exciton model. Kolosyuk, Vashchenko, and Berezdetskii[9] also observed a large shift of the direct edge at room temperature in low magnetic fields. A much smaller shift of the edge at 77 K was detected in the present experiment even by an application of seven times stronger magnetic field than their experiment. Therefore, there should be some error in their analysis of the experimental result. The present results of small effects of magnetic fields on excitons in BiI_3 show that the effect cannot be analyzed by a relative motion of Wannier excitons based on the effective-mass approximation but by the Zeeman effect of the cationic excitons having small radii. The present success in measuring the magneto-optical effect in the Urbach tail suggests a useful method to investigate the excitons having very strong absorption coefficients avoiding the difficulty of preparing very thin samples.

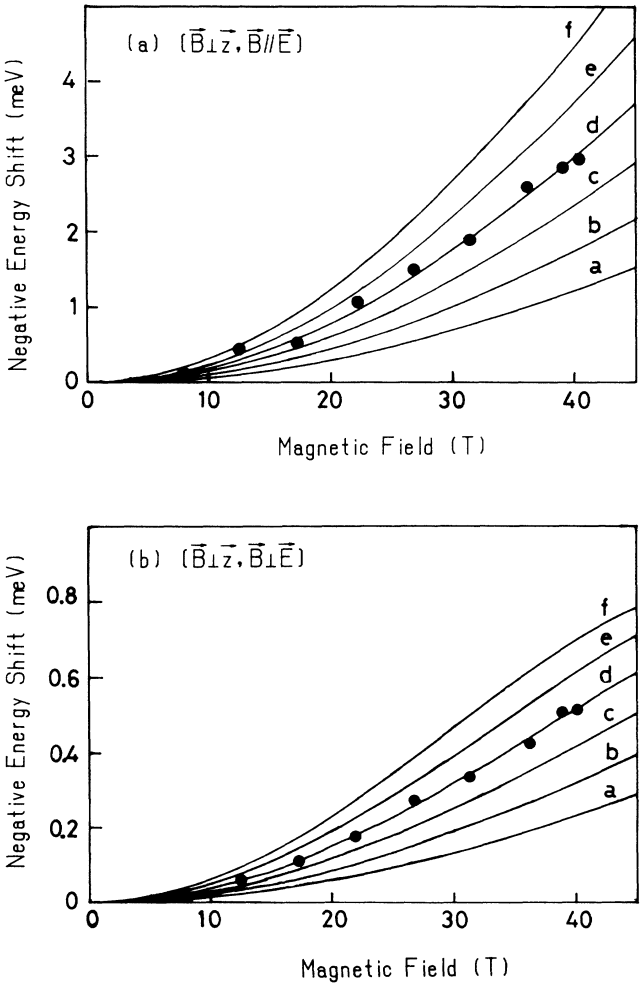

FIG. 12. Magnetic-field dependence of energy shifts of the Urbach tail in the (a) $\mathbf{B}\|\mathbf{E}$ and (b) $\mathbf{B}\perp\mathbf{E}$ configurations. The ordinate shows values of shifts to the lower-energy side. Solid circles show the experimental values. Solid lines are calculated assuming the values of the $g_{\text{eff}}^{\perp}$: *a*, 1.0; *b*, 1.2; *c*, 1.4; *d*, 1.6; *e*, 1.8; *f*, 2.0.

V. CONCLUSION

The magneto-absorption spectra of both the indirect exciton and the Urbach tail of the direct exciton transitions at the band-edge region in BiI_3 have been measured in pulsed high magnetic fields. From the first successful magneto-optical measurement on the Urbach tail in BiI_3, the magnetic-field effect of the direct exciton was clarified. The observed magnetic-field-induced indirect exciton enabled precise line-shape analyses and comparisons with the zero-field indirect exciton. A remarkable anisotropy was observed with respect to the magnetic field direction of an incident light. Drastic changes of the spectra by magnetic fields were observed especially for the $\mathbf{B}\perp\mathbf{z}$ configuration, reflecting the dominating role of the Zeeman term in this exciton system. The value of $g_{\text{eff}}^{\perp}$ was determined both for the direct and the indirect excitons, while the value of $g_{\text{eff}}^{\|}$ was at least one order of magnitude smaller than that of the $g_{\text{eff}}^{\perp}$. A characteristic energy shift with B^2 dependence and a growth of a new transition with B^2 dependence were commonly observed for these exciton transitions. The energy position of the triplet exciton state was determined for the indirect exciton state. The large exchange, Coulomb, and spin-orbit interactions of these excitons were found to be more important than the relative motion of the excitons for the magnetic-field effect, which is explained not by a usual Wannier exciton model based on the effective-mass approximation, but mainly by the cationic exciton model having small radii in BiI_3.

ACKNOWLEDGMENTS

The authors would like to thank Professor T. Iida for his kind discussion through this work from the theoretical point of view. They are also indebted to Professor Y. Toyozawa for the encouragements through this work. This work was partially supported by Grant-in-Aid for Scientific Research from the Ministry of Education, Science and Culture in Japan.

---

*Permanent address: Department of Physics, Faculty of Liberal Arts and Education, Yamanashi University, Takeda, Kofu 400, Japan.

[1]D. C. Reynolds and T. C. Collins, in *Excitons, Their Properties and Uses* (Academic, New York, 1981), pp. 8–31.

[2]K. Cho, S. Suga, W. Dreybrodt, and F. Willmann, Phys. Rev. B **11**, 1512 (1975).

[3]R. W. G. Wyckoff, in *Crystal Structures* (Interscience, New York, 1960), Vol. 2, p. 12.

[4]T. Komatsu, Ph.D. thesis, Osaka City University, 1982.

[5]Y. Kaifu and T. Komatsu, J. Phys. Soc. Jpn. **40**, 1377 (1976).

[6]Y. Kaifu, J. Lumin. **42**, 61 (1988).

[7]I. Ch. Schluter and M. Schluter, Phys. Rev. B **9**, 1652 (1974).

[8]T. Komatsu and Y. Kaifu, J. Phys. Soc. Jpn. **40**, 1061 (1976).

[9]V. N. Kolosyuk, V. I. Vashchenko, and T. I. Berezdetskii, Opt. Spectrosk. **39**, 600 (1975).

[10]T. Komatsu, Y. Kaifu, S. Takeyama, and N. Miura, Phys. Rev. Lett. **58**, 2259 (1987).

[11]K. Watanabe, T. Komatsu, S. Takeyama, Y. Iwasa, N. Miura, and Y Kaifu, J. Phys. C **20**, 6315 (1987).

[12]M. Schiebr, T. J. Davies, W. F. Schnepple, P. R. Randtke, and R. C. Carlston, J. Appl. Phys. **45**, 5371 (1974).

[13]N. Miura, T. Goto, K. Nakao, S. Takeyama, T. Sakakibara, and F. Herlach, J. Magn. Magn. Mater. **54-57**, 1409 (1986).

[14]T. Karasawa, T. Komatsu, and Y. Kaifu, Solid State Commun. **44**, 323 (1982).

[15]J. C. Slater, in *Quantum Theory of Molecules and Solids* (McGraw-Hill, New York, 1965), Vol. 2, p. 424.

[16]T. Iida, M. Sakai, T. Karasawa, T. Komatsu, and Y. Kaifu, J. Phys. C **16**, 4719 (1983).

[17]T. Karasawa, K. Miyata, T. Komatsu, and Y. Kaifu, J. Phys. Soc. Jpn. **52**, 2592 (1983).